Cortical Constraint Method for Diffuse Optical Brain Imaging

Misha E. Kilmer[a], Eric L. Miller[b], Marco Enriquez[a], David Boas[d]

[a]Mathmatics Department, Tufts University, Medford, MA, USA;
[b]ECE Department, Northeastern University, Boston, MA, USA;
[d] Anthinoula A. Martinos Center for Biomedical Imaging, Massachusetts General Hospital, Harvard Medical School, Charlestown, MA, USA

ABSTRACT

We develop a parametric, shape-based image reconstruction algorithm for the joint reconstruction of the optical absorption and diffusion coefficients in the brain using diffuse optical tomographic data. Specifically, we study the recovery of the geometry of an unknown number of 2D closed contours located on a 2D manifold (the cortex) in 3-space. We describe an approach for a brain model in which we assume the existence of a one-to-one map from the surface of the cortex to a subset of the plane. We use a new, parametric level set approach to map shapes on the plane to structures on the cortex. Our optimization-based reconstruction algorithm evolves shapes on the plane while finding absorption and reduced scattering values inside each shape. Preliminary numerical simulation results show the promise of our approach.

Keywords: tomography, DOT, parametric, shape-based, image reconstruction, absorption, diffusion

1. INTRODUCTION

Diffuse optical tomographic (DOT) brain imaging makes use of modulated, near-infrared light transmitted into the head from photodiodes placed on the scalp. Optical detectors then measure the photon fluence resulting from the scattering and absorption of photons within the brain. Because these interactions are governed by the oxygenation of the brain tissue, reconstructing the spatial and temporal distributions of scattering and absorption properties of the tissue from diffuse optical measurements has recently shown promise as a means of functional brain imaging.[1–3]

The goal is to use the measured photon fluence at the detectors on the scalp to generate three-dimensional images of the absorption coefficient, $\mu_a(r)$ and diffusion coefficient $D(r)$ (which is inversely proportional to the reduced scattering coefficient, $\mu_{s'}(r)$), within some region of interest in the brain. In this paper, we consider only imaging using data obtained in the temporal frequency domain and a linear forward model. Unfortunately, the limited-view nature of this problem makes the stable recovery of the 3D distribution of the optical properties of the brain very sensitive to noise in the data. Furthermore, the amount of data is small relative to the total number of voxel values that must be recovered. Thus, a least squares approach to recovering the images of absorption and diffusion is inadequate as the least squares problem is both underdetermined and ill-posed. Some form of regularization must be employed. Two of the most well-known regularization methods when linear forward models are employed are Tikhonov regularization and truncated singular value decomposition (TSVD).[4] Besides the difficult problem of choosing regularization parameters to determine the reconstructions for any of these methods, when applied to the full three-dimensional image reconstruction problem, the methods are computationally expensive.

In the last several years, parameterized imaging methods have been used for reconstruction of optical images[5–9] in two and three dimensions. The idea behind these methods is that the unknown absorption and diffusion are modeled as a collection of a known number of anomalies whose shape, location and characteristics are unknown. The shapes are parameterized by some method. The reconstruction problem then becomes one of recovering the parameters that define the boundaries of the anomalies and the values inside,[5–9] and perhaps the values of expansion coefficients that determine the background values of the optical properties as well.[5, 6]

Further author information: Send correspondence to Misha Kilmer (misha.kilmer@tufts.edu)

These types of parameterization approaches have the advantage of reducing the dimension of the search space, and therefore the computational expense, of the reconstruction.

Shape-based, parameterized reconstruction methods have been observed to have the additional advantage of imposing regularization directly through the model itself so that the inversion does not require additional regularization to recover solutions.[6,9] This is due to the fact that optimization problem is over-determined, rather than under-determined, and the solutions are constrained to conform to the model. For example, in,[6] the authors used ellipsoids to model the anomalies in 3D breast imaging for DOT. The reconstruction problem under this assumption became one of determining the ellipsoid descriptors (axis length, orientation, and center location) as well as the expansion coefficients that would determine the values of absorption inside and outside the ellipsoid. A least-squares approach was then used to determine both the expansion coefficents and shape descriptors, and no additional regularization was needed.

In this paper, we explore a shaped-based, parameterized reconstruction specific to 3D DOT brain imaging that allows for flexible models of shape. In particular, we exploit two pieces of prior information regarding the optical properties in the brain. First, it is known that the types of functional activity in the brain for which DOT is intended are geometrically restricted to lie on the cortex, a region of the brain which is essentially a two-dimensional surface. Second, functional regions are modeled as a collection of piecewise constant "hot-spots" bounded by closed curves on the cortex. Thus we study the recovery of the geometry of an unknown number of 2D closed contours located on a 2D manifold (the cortex) in 3-space.

We describe an approach for a brain model in which we assume the existence of a one-to-one map from the surface of the cortex to a subset of the plane. We use a new, parametric level set approach to map shapes on the plane to structures on the cortex. Our optimization-based algorithm evolves shapes on the plane while finding absorption values inside each shape.

This paper is organized as follows. In Section 2, we give the mathematical background regarding the reconstruction problem. We describe our imaging algorithm based on our shape-based model in Section 3. We present the results of two numerical simulations in Section 4 and finish with conclusions and future work in Section 5.

2. BACKGROUND

Mathematically, the model we use to describe the relation between the photon fluence and the absorption and/or reduced scattering coefficients $\mu_a(r), \mu_{s'}(r)$ is the linear first-Born approximation.[10] Let $\delta\mu_a(r)$ denote the perturbation of $\mu_a(r)$ about some constant known background value. Now the relation of the diffusion coefficient $D(r)$ to the reduced scattering coefficient is $1/(3\mu_{s'}(r))$. For our model, it is more convenient to image for the perturbation to the diffusion coefficient, $\delta D(r)$, about a known background value than it is to image for the perturbation to the reduced scattering function directly. Thus, given near-infared light modulated at a frequency of ω Hz, a source at position r_s, and detector at position r_d we have

$$q(r_d) = \int_\Omega G_\omega(r_d, r')G_\omega(r', r_s)\delta\mu_a(r')dr' + n(r_d) \tag{1}$$

if scattering is ignored and

$$q(r_d) = \int_\Omega [G_\omega(r_d, r')G_\omega(r', r_s)\delta\mu_a(r') + \nabla_{r'}G_\omega(r_d, r') \cdot \nabla_{r'}G_\omega(r', r_s)\delta D(r')]dr' + n(r_d) \tag{2}$$

if scattering and absorption are both accounted for. Here, $y(r_d)$ denotes the "data" (the difference between the input source and the measured output) corresponding to the detector located at position r_d. The term $n(r_d)$ is used to model the noise at position r_d and G_ω denotes the Green's function in the medium which is constructed assuming fixed background values for the absorption and reduced scattering coefficient and a δ-function source at position r_s.

Technically speaking, Ω in (1) and (2), is the entire three-dimensional region of the brain in which the region to be imaged lies. However, as noted in the introduction we are assuming that the fuctional activity is restricted to the cortex, an essentially two-dimensional region. Therefore, the perturbations $\delta\mu_a(r), \delta D(r)$ have support only over the surface of the cortex.

We discretize (1) and (2) at each of a fixed number of frequencies, ω_k, $k = 1, \ldots, K$ using a method of moments approach using pulse basis functions.[11] For a fixed frequency ω_k and over all sources and detectors, this gives the matrix equations

$$b^{(k)} = (A^{(k)} + iB^{(k)})f_a + n^{(k)} \tag{3}$$

for (1) and

$$b^{(k)} = (A^{(k)} + iB^{(k)})f_a + (C^{(k)} + iE^{(k)})f_s + n^{(k)} \tag{4}$$

where f_a, f_s are the discretized versions of $\delta\mu_a$ and δD, respectively. However, since f_a and f_s are known to be real, these matrix equations can be more consisely written in block form, stacking equations for all frequencies, as

$$\begin{bmatrix} b_R^{(1)} \\ b_I^{(1)} \\ \vdots \\ b_R^{(K)} \\ b_I^{(K)} \end{bmatrix} = \begin{bmatrix} A^{(1)} \\ B^{(1)} \\ \vdots \\ A^{(K)} \\ B^{(K)} \end{bmatrix} f_a + \begin{bmatrix} n_R^{(1)} \\ n_I^{(1)} \\ \vdots \\ n_R^{(K)} \\ n_I^{(K)} \end{bmatrix},$$

using (3) and

$$\begin{bmatrix} b_R^{(1)} \\ b_I^{(1)} \\ \vdots \\ b_R^{(K)} \\ b_I^{(K)} \end{bmatrix} = \begin{bmatrix} A^{(1)} & C^{(1)} \\ B^{(1)} & E^{(1)} \\ \vdots & \\ A^{(K)} & C^{(K)} \\ B^{(K)} & E^{(K)} \end{bmatrix} \begin{bmatrix} f_a \\ f_s \end{bmatrix} + \begin{bmatrix} n_R^{(1)} \\ n_I^{(1)} \\ \vdots \\ n_R^{(K)} \\ n_I^{(K)} \end{bmatrix},$$

using (4).

In either case, we use b to denote the stacked data vector, A to denote the stacked matrix, and f to denote the desired vector. The unregularized, least squares problem is

$$\min_f \|W(b - Af)\|_2, \tag{5}$$

where W is a weighting matrix determined by the noise characteristics to be described later. As noted in the introduction, this problem is both underdetermined and very sensitive to noise in the data. The Tikhonov approach would be to solve the regularized problem

$$\min_f \|W(b - Af)\|_2^2 + \lambda^2\Gamma(f),$$

where λ is a regularization parameter that is usually difficult to determine and $\Gamma(f)$ is a regularization operator. There are of course many different types of conventional regularization methods that could be employed (see for example[4]). However, we will consider a fundamentally different approach. As we see in the next section, the regularization is, together with an appropriate stopping criteria, a part of the model we employ for f.

3. MODEL AND ALGORITHM

Recall from the Introduction that there are two assumptions we make use of for DOT brain imaging. In our discretization, we have already assumed that the perturbations in absorption and diffusion have support only over the cortex. We now assume that there exists a one-to-one mapping from the cortex to points in a plane in $\mathbb{R}^2$. In particular, let $h(x, y)$ describe the surface of the brain as a function of the spatial variables (x, y) in the plane. For simplicity, we assume that $(x, y) \in [-1, 1] \times [-1, 1]$, so that $h(x, y)$ gives the height of the cortical surface above the plane. We give an example of a simple brain mock-up according to this model in Figure 1. Therefore, in the discretization of (1, (2), we descretize at the points $r_{m,n} = (x_m, y_n, h(x_m, y_n))$, for $x_m = -1 + \Delta m, m = 0, \ldots, M - 1$, $y_n = -1 + \Delta n, n = 0, \ldots, M - 1$.

Under the assumption that the surface of the cortex corresponds to the one-to-one function $h(x, y)$, we are now in a position to talk about evolving shapes on the surface of the cortex. We would like to model, as closely

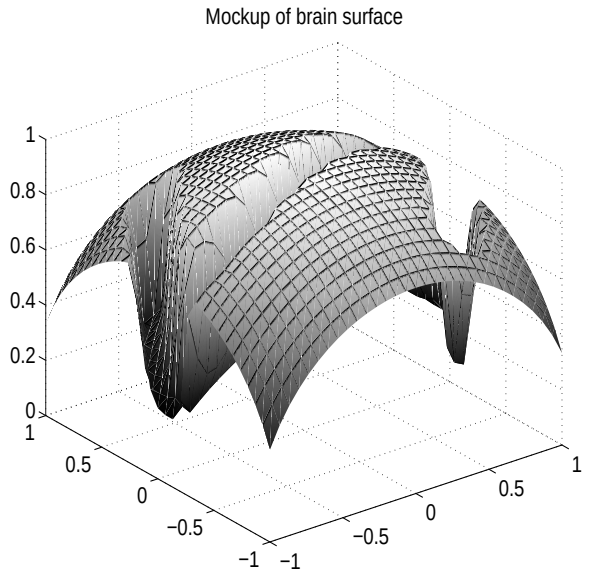

Figure 1. Mockup of brain used in numerical experiments section.

as possible, the case that the perturbations $\delta\mu_a(r), \delta D(r)$ are piecewise constant. That is, these functions should have a particular value inside anomalies (which we are representing as the evolving shapes), and be zero outside. The key point is that since $h(x, y)$ is one-to-one, evolving shapes on the surface of the cortex is equivalent to evolving shapes in the box $[-1, 1] \times [-1, 1]$ on the $x - y$ plane. First, consider the function

$$g(x, y) = \alpha(1/2 + 1/2(\tanh(-\beta p(x, y)))),$$

where $p(x, y)$ is assumed to be any fixed-degree polynomial in the two variables x, y. For example, if the degree is two,

$$p(x, y) = a_{0,0} + a_{1,0}x + a_{0,1}y + a_{2,0}x^2 + a_{1,1}xy + a_{0,2}y^2.$$

We consider the scalar α and the polynomial coefficients $a_{i,j}$ to be the unknowns in this case, while β is a known, positive, parameter (in our case, $\beta = 30$. The function $g(x, y)$ is bounded above by α and below by zero. In effect, the function $(0.5 + .5(\tanh(-\beta p(x, y)))$ models the Heaviside function. It should be close to 1 as the argument $-\beta p(x, y) \geq \pi$ and close to 0 when the argument is $\leq -\pi$. One nice feature of $g(x, y)$ is that it is differentiable with respect to all the unknowns. We can certainly model circles and ellipses in the plane with this approach, but we can also model more interesting shapes (and more than one shape) by using higher degree polynomials. In our experiments, we use polynomials of degree 4 (in which case there are 15 coefficients).

We assume that both absorption and scattering can be modeled using this approach: namely, that

$$\delta\mu_a(r) = \alpha_a(1/2 + 1/2(\tanh(-\beta p(x, y)))), \qquad \text{for } r = (x, y, h(x, y)),$$

and

$$\delta D(r) = \alpha_s(1/2 + 1/2(\tanh(-\beta \tilde{p}(x, y)))), \qquad \text{for } r = (x, y, h(x, y)),$$

for two polynomials $p(x, y), \tilde{p}(x, y)$, of possibly different degrees and coefficients.

Recall that f represents the vectorized form of the absorption (or stacked absorption, diffusion) perturbation images. Now that the optical properties are defined in terms of scalars and polynomial coefficients, the optimization problem we wish to solve (compare to (5)) becomes the weighted least squares problem

$$\min_v \|W(y - Af(v))\|_2^2 = \epsilon(v)^T \epsilon(v) \tag{6}$$

where v denotes the vector containing the unknowns $\alpha_a, a_{i,j}$ (as well as $\alpha_s, \tilde{a}_{i,j}$ if the diffusion perturbation is also to be solved for), and ϵ denotes the residual vector $Wy - WAf(v)$. Clearly, this problem is better posed than (5) because, if the polynomial degree is not too high, there are fewer unknowns and the structure of the solution is enforced through the model.

This optimization problem is a non-linear least-squares problem. We use a Levenberg-Marquardt algorithm to determine the optimal set of parameters v.[12] As we will discuss in the next section, we use the MATLAB procedure `lsqnonlin` from the MATLAB Optimization Toolbox to solve the problem. To run the algorithm, we only need to supply a subroutine that computes $\epsilon(v)$ and evaluates the Jacobian of ϵ with respect to v. Because there is noise in the data vector y, we do not wish to force the residual vector to be too small in norm. In fact, ideally, we should stop iterating when $\|\epsilon\|_2^2 \approx \|Wn\|_2^2$. This idea of stopping the iteration when the norm of the residual is proportional to an estimate of the norm of the noise vector, is known as the Discrepancy Principle.[4] In our examples, however, the algorithm would usually slow down significantly (i.e. $\|\epsilon(v_k)\|_2$ did not change much in a relative sense from one iteration to the next) near the value $\|Wn\|_2^2$ so that we would just iterating once this value was reached and after this slow-down began.

4. NUMERICAL RESULTS

All experiments were conducted in IEEE double precision floating point arithmetic in MATLAB with the MATLAB Optimization Toolbox. Both experiments were carried out using data obtained at two, non-zero frequencies: $\omega_1 = 30$ MHz and $\omega_2 = 70$ MHz. The background values for μ_a and $\mu_{s'}$ used to construct the matrices where 5 m^{-1} and 1000 m^{-1}, respectively. In this problem, the speed of light in the medium (needed to construct the matrices) was $\nu = 3 \times 10^8/1.4$ m/s. The background diffusion coefficient was $1/(3 \times 1000)$ meters. In the discretization, $\Delta = 1/15$, thereby dividing the planar region $[-1, 1] \times [-1, 1]$ into a 31×31 grid. The sources and detectors are arranged on the surface of our simulated head as displayed in Figure 2.

We used the same model to generate our data as we did to invert the data. In both experiments, the degrees of the polynomials used in the inversion and in data generation was 4. We took $\beta = 30$. To generate the noise, we used a different Gaussian white noise for each subvector $n_I^{(k)}$ and $n_R^{(k)}$, $k = 1, 2$. The noise subvectors were determined using the `randn` function in MATLAB and scaled so that the ratio, in the 2-norm, of the noise subvector to the corresponding true signal subvector, was some predetermined number $c \times 10^{-2}$. Thus, in our experiments, there were four different values whitenoise subvectors, each with a different standard deviation. We set W to be the diagonal matrix containing the reciprocal of each of these standard deviations along the diagonal; that is, W had only four distinct values along its main diagonal. This gave a noise-to-signal ratio, defined as $\|Wn\|_2/\|Wy_{true}\|_2$ where y_{true} denotes the noise-free signal, of c percent. We set the maximum number of iterations by hand to try to force the algorithm to stop iterating when $\|\epsilon\|_2^2 \approx \|Wn\|_2^2$.

Of course, the Levenberg-Marquardt algorithm requires a starting guess at the parameters of unknowns. We assume that we know nothing a priori about the location of the anomaly (anomalies). So the initial polynomial coefficients are selected so that the initial shape, as projected on the plane, whether for absorption or diffusion perturbation, looks like a circle with radius 1. This shape is given in Figure 3. However, a starting guess for the scalar(s) $\alpha_a(\alpha_b)$ must be also be determined. To determine this starting guess, we ran the Levenberg-Marquardt algorithm, with the polynomial coefficients fixed as described, to find the estimated value of $\alpha_a(\alpha_b)$ that was optimal for this initial shape. Then, we call Levenberg-Marquardt using the initial shape and estimated $\alpha_a(\alpha_b)$.

4.1. Example 1

In this example, we ignore absorption and invert for the perturbation of the diffusion coefficient only. To generate the true data, $\alpha_a = 30$. The noise to signal ratio was 5 percent. On the first call to Levenberg-Marquardt, we took the guess of $\alpha_a = 5$, which corresponds to was the known background value of 5 m^{-1}. On the second call to Levenberg-Marquardt, where we optimize over all the unknowns, we stopped after 100 iterations, as this was the point at which $\|\epsilon\|_2^2 \approx \|Wn\|_2^2$ and convergence had slowed down considerably.

The three dimensional image of the true absorption is shown in the top row of Figure (4 and the reconstructed image in the top right of the figure. (We ran this experiment for several different noise realizations, and the results were always consistent we those we display here.) For further comparison, we show the projection of

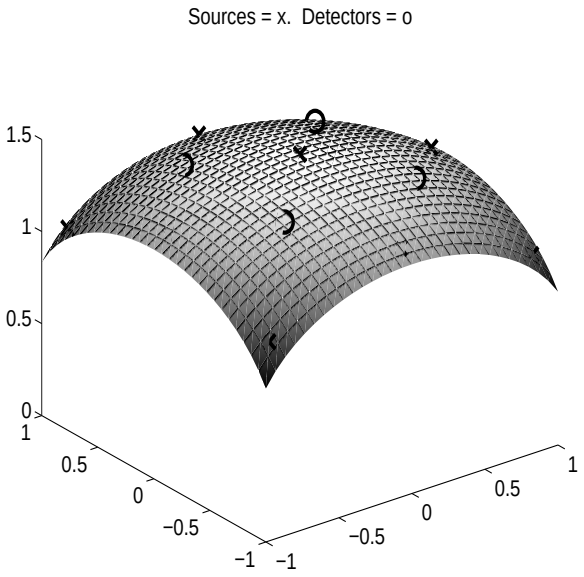

Figure 2. Location of sources and detectors.

the true and reconstructed images onto the plane in bottom row of Figure 4. Clearly, even with a 5 percent noise-to-signal ratio, these reconstructions are good at localization and characterization of the anomaly.

4.2. Example 2

Since we are using a polynomial of degree 4 in our examples, we are also able to model and capture situations where the absorption is comprised of disjoint sections. In this example, the true value of α_a was 20. The pictures

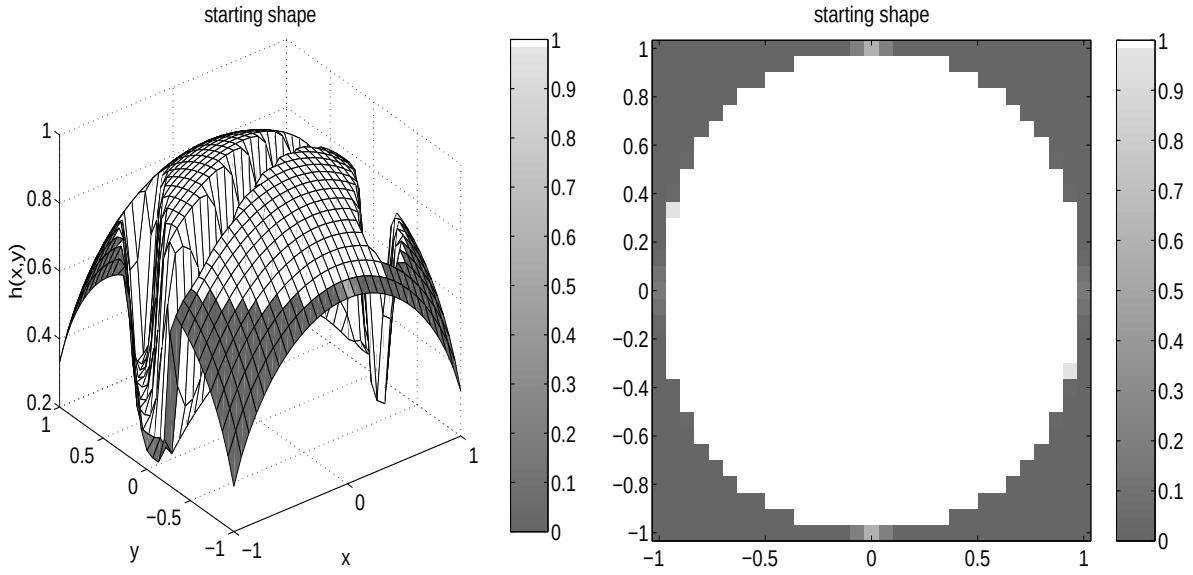

Figure 3. Left: initial shape guess as it appears on the surface of the brain. Right: initial shape as it appears on the plane.

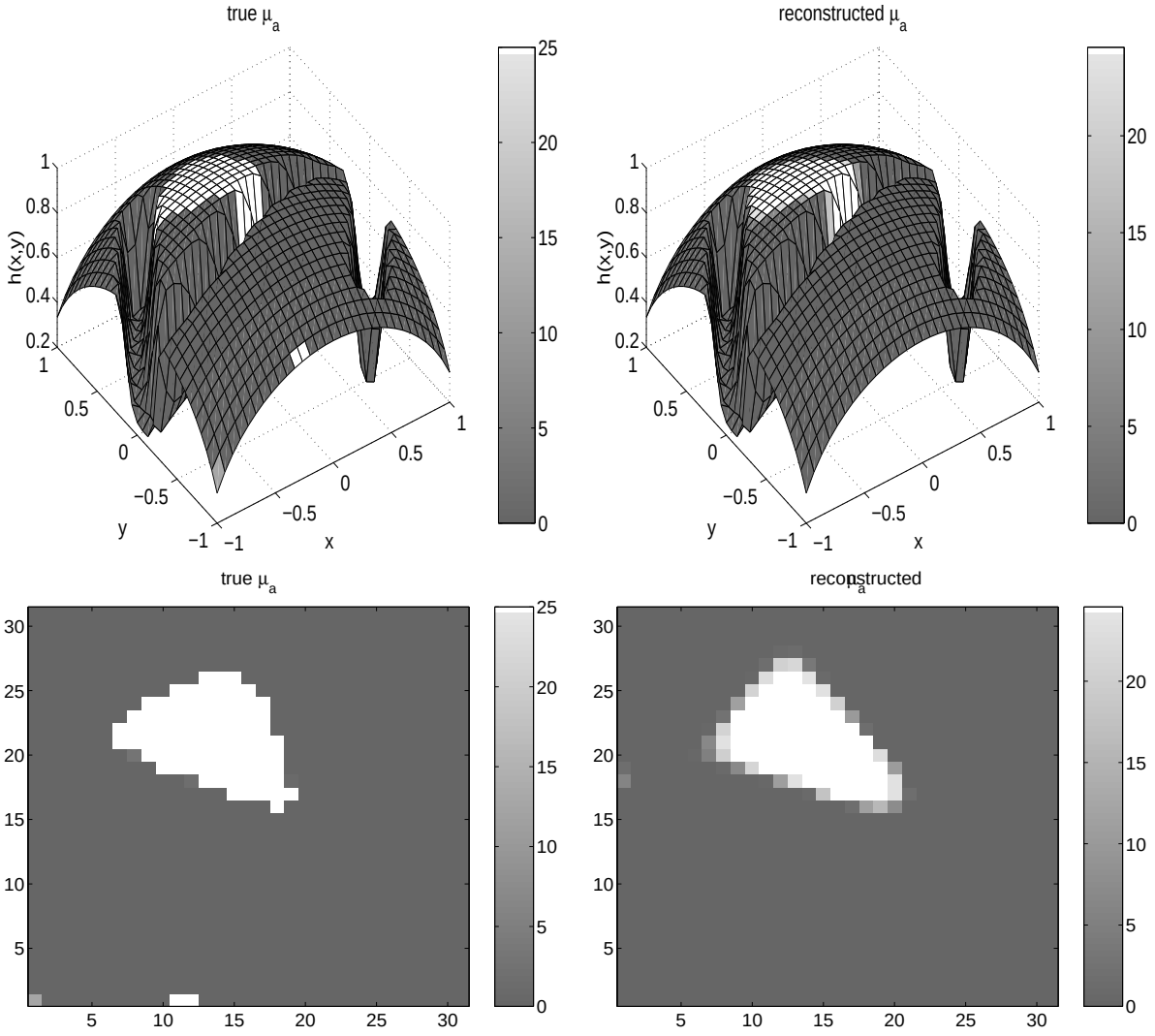

Figure 4. Example 1. Top left: True, 3D absorption perturbation image; Top right: 3D reconstruction; Bottom left: True image as it appears in the plane; Bottom Right: Reconstruction as it appears in the plane.

in Figure 5 show that even for a noise-to-signal ratio of as high as 10 percent, after running 125 LM iterations using the same starting guess as Example 1, our approach is able to capture this behavior fairly well.

4.3. Example 3

In this example, we image jointly for the absorption and diffusion coefficients. The true value for α_a was 30. We set the true value for α_b to be $1/(3 \times 200) - 1/(3 \times 1000)$. Since the actual differences in the absorption and diffusion perturbations was several orders of magnitude, we pre-scaled the true solution and starting guess by a factor c to bring the true diffusion magnitude to 25. We then "un-scaled" by multiplying the second block column of the matrix in (4) by the factor $1/c$. Note that this has no effect on the generation of the data, but it may help improve the calculation of search directions by the optimization algorithm.

We used a 1 percent noise-to-signal ratio in this example. Notice from the true images displayed in the first row of Figure 6 that the absorption and diffusion anomalies are not co-located.

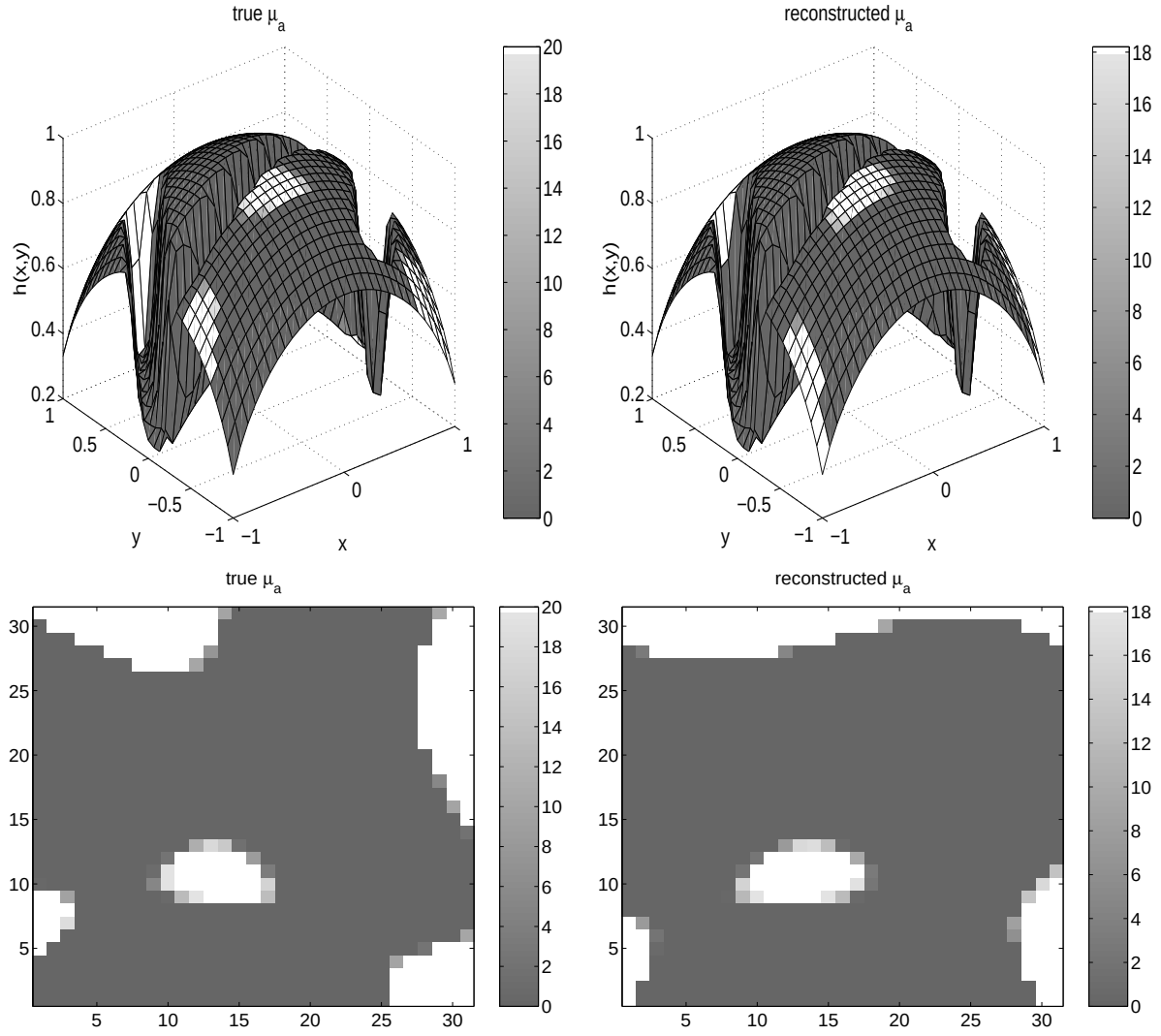

Figure 5. Example 2. Top left: True, 3D absorption perturbation image; Top right: 3D reconstruction; Bottom left: True image as it appears in the plane; Bottom Right: Reconstruction as it appears in the plane.

We used the same starting guess shapes for both images, and we ran the Levenberg-Marquardt algorithm on the smaller problem with initial guesses $\alpha_a = 5$, $\alpha_b = 1/(3 \times 1000)$ (corresponding to the background values of $\mu_a, \mu_{s'}$ used to construct the Green's function matrices) to determine values that were optimal for this fixed shape. Then we ran Levenberg-Marquardt on the full problem, optimizing for polynomial coefficients for both shapes as well as scalar coefficients α_a and α_b. The reconstructions of both coefficients after 100 Levenberg-Marquardt iterations are displayed in Figure 7. Both reconstructions show good localization and characterization, particularly given the poor quality of the initial guess.

5. CONCLUSIONS AND FUTURE WORK

We have presented a model and corresponding algorithm for 3D cortical imaging of the absorption and diffusion coefficients. Our approach has the advantage of reducing the computational complexity of the 3D image problem by effectively reducing it to a 2D imaging problem. Additionally, our method has the benefit of having regularization that is built-in through the model. Numerical results indicate the promise of this approach.

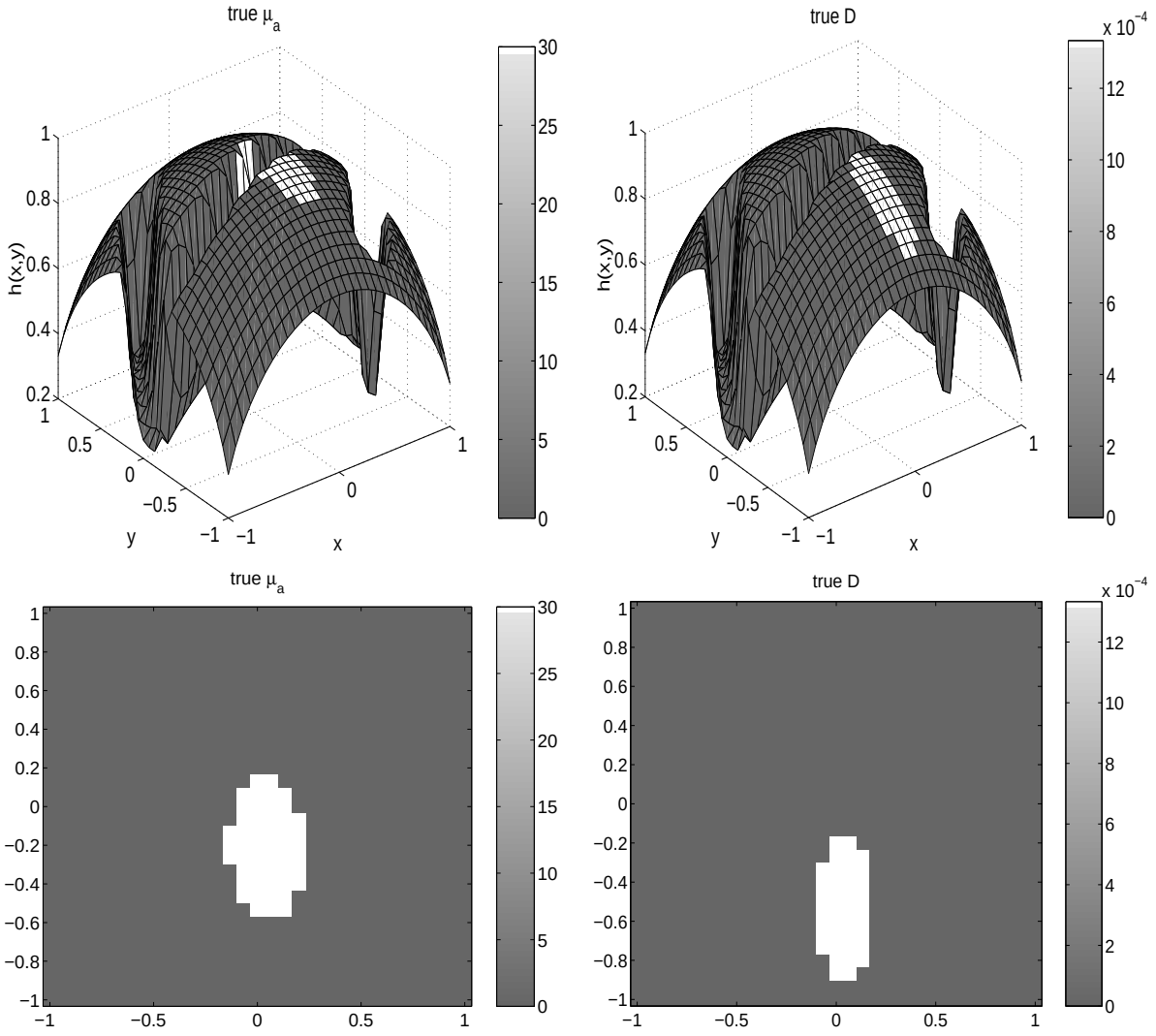

Figure 6. Example 3. Left column: True absorption perturbation image on the cortex (top) and projected onto the plane (bottom). Right column: True diffusion perturbation image on the cortex (top) and projected onto the plane (bottom).

In future work, it is necessary to consider imaging for more than one anomaly where those anomalies may have different weighting coefficients. A small change in our model will also allow for background values to be recovered if we assume the exact background absorption and scattering coefficients are not known a priori. In the future, we will consider more realistic brain models and apply our results to clinical data.

ACKNOWLEDGMENTS

Work on this research was supported by the National Science Foundation through NSF Grants 0139968 and 0208548.

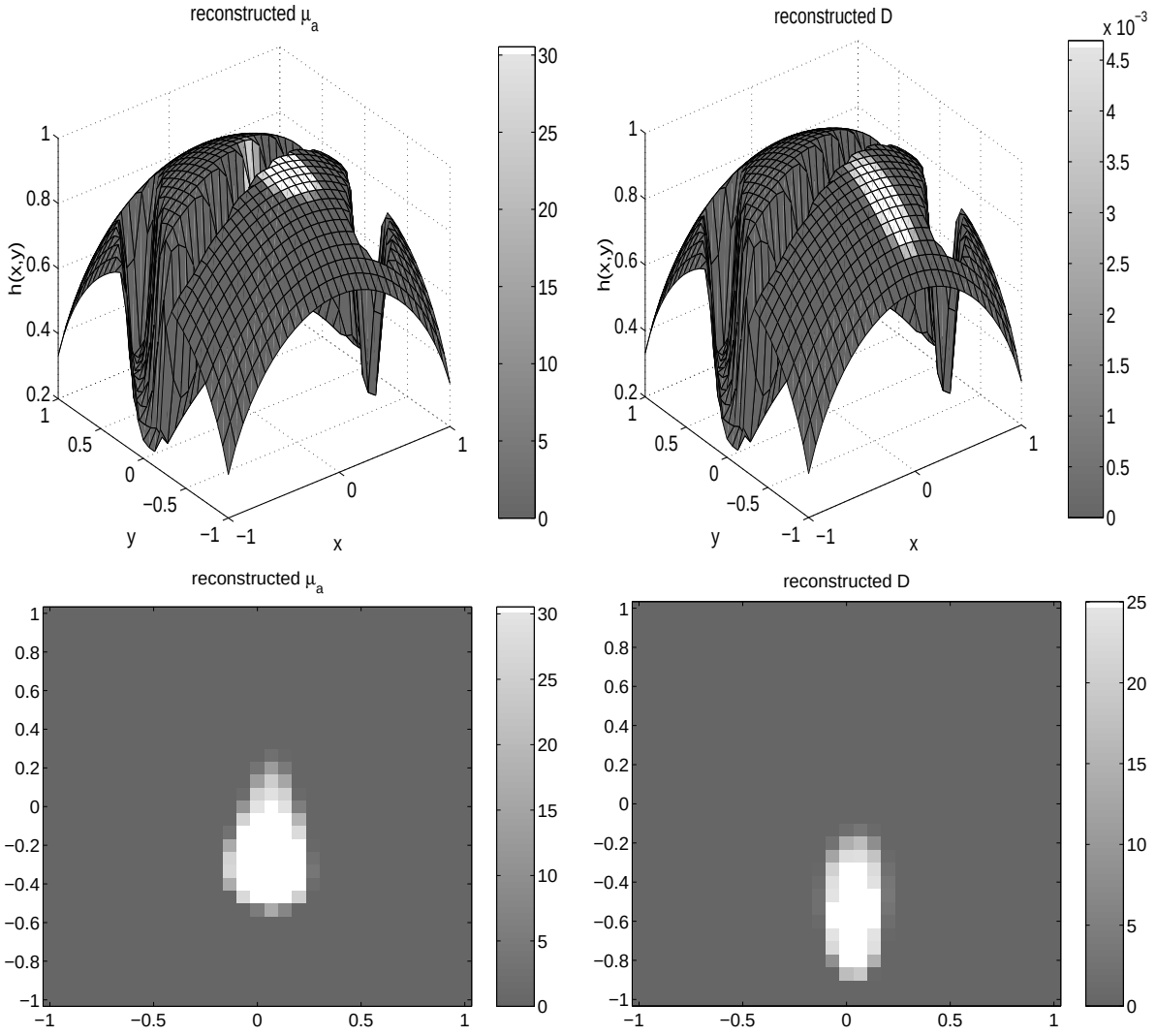

Figure 7. Example 3. Left column: Reconstructed absorption perturbation image on the cortex (top) and projected onto the plane (bottom). Right column: Reconstructed reduced diffusion perturbation image on the cortex (top) and projected onto the plane (bottom).

REFERENCES

1. J. Hebden, A. Gibson, T. Austin, R. M. Yusof, N. Everdell, D. Delpy, S. Arridge, J. Meek, and J. Wyatt, "Imaging changes in blood volume and oxygenation in the newborn infant brain using three-dimensional optical tomography," *Physics in Medicine and Biology* **49**, pp. 1117–1130, 2004.
2. A. Siege, J. Culver, J. Mandeville, and D. Boas, "Temporal comparison of functional brain imaging with diffuse optical tomography and fmri during rat forepaw stimulation," *Physics in Medicine and Biology* **48**, pp. 1391–1403, 2003.
3. J. Culver, A. Siegel, J. Stott, and D. Boas, "Volumetric diffuse optical tomography of brain activity," *Optics Letters* **28**, 2003.
4. P. C. Hansen, *Rank Deficient and Discrete Ill-Posed Problems*, SIAM Press, Philadelphia, 1998.
5. M. Kilmer, E. Miller, A. Barbaro, and D. Boas, "3D shape-based imaging for diffuse optical tomography," *Applied Optics* **42**, pp. 3129–3144, 2003.

6. M. Kilmer, E. Miller, D. Boas, and D. Brooks, "A shape-based reconstruction technique for DPDW data," *Optics Express* **7**, pp. 482–491, 2000.
7. E. Miller, A. Hamdi, D. Keesing, M. Kilmer, M. Franceschini, and D. Boas, "Recursive estimation methods for tracking of localized perturbations in absorption and scattering using diffuse optical tomography," in *Proceedings of the SPIE: Computational Imaging II*, 2004. Vol. 5299.
8. V. Kolehmainen, S. Arridge, W. Lionheart, M. Vauhkonen, and J. Kaipio, "Recovery of region boundaries of piecewise constant coefficients of an elliptic pde from boundary data," *Inverse Problems* **15**, pp. 1375–1391, 1999.
9. V. Kolehmainen, M. Vauhkonen, J. Kaipio, and S. Arridge, "Recovery of piecewise constant coefficients in optical diffusion tomography," *Optics Express* **7**, pp. 468–480, 2000.
10. S. Arridge, "Optical tomography in medical imaging," *Inverse Problems* **15**, pp. R41–R93, 1999.
11. R. Harrington, *Field Computation by Moment Methods*, Macmillan, New York, 1968.
12. M. Heath, *Scientific Computing: An Introductory Survey*, McGraw Hill, New York, second ed., 2002.